nature COMMUNICATIONS

ARTICLE

Received 11 Dec 2013 | Accepted 29 Jan 2014 | Published 17 Feb 2014

DOI: 10.1038/ncomms4342

Direct synthesis of single-walled aminoaluminosilicate nanotubes with enhanced molecular adsorption selectivity

Dun-Yen Kang[1,2], Nicholas A. Brunelli[1,3], G. Ipek Yucelen[4], Anandram Venkatasubramanian[5], Ji Zang[1], Johannes Leisen[6], Peter J. Hesketh[5], Christopher W. Jones[1,6] & Sankar Nair[1]

Internal functionalization of single-walled nanotubes is an attractive, yet difficult challenge in nanotube materials chemistry. Here we report single-walled metal oxide nanotubes with covalently bonded primary amine moieties on their inner wall, synthesized through a one-step approach. Conclusive molecular-level structural information on the amine-functionalized nanotubes is obtained through multiple solid-state techniques. The amine-functionalized nanotubes maintain a high carbon dioxide adsorption capacity while significantly suppressing the adsorption of methane and nitrogen, thereby leading to a large enhancement in adsorption selectivity over unfunctionalized nanotubes (up to four-fold for carbon dioxide/methane and ten-fold for carbon dioxide/nitrogen). The successful synthesis of single-walled nanotubes with functional, covalently-bound organic moieties may open up possibilities for new nanotube-based applications that are currently inaccessible to carbon nanotubes and other related materials.

[1] School of Chemical & Biomolecular Engineering, Georgia Institute of Technology, 311 Ferst Drive NW, Atlanta, Georgia 30332, USA. [2] Department of Chemical Engineering, National Taiwan University, No. 1, Sector 4, Roosevelt Road, Taipei 10617, Taiwan. [3] Department of Chemical and Biomolecular Engineering, The Ohio State University, 125A Koffolt Laboratories, 140 West 19th Avenue, Columbus, Ohio 43210, USA. [4] School of Materials Science and Engineering, Georgia Institute of Technology, 771 Ferst Drive NW, Atlanta, Georgia 30332, USA. [5] G.W. Woodruff School of Mechanical Engineering, Georgia Institute of Technology, 801 Ferst Drive NW, Atlanta, Georgia 30332, USA. [6] School of Chemistry and Biochemistry, Georgia Institute of Technology, 901 Atlantic Drive NW, Atlanta, Georgia 30332, USA. Correspondence and requests for materials should be addressed to C.W.J. (email: cjones@chbe.gatech.edu). or to S.N. (email: sankar.nair@chbe.gatech.edu).

Single-walled nanotubes ('SWNTs') are important 'building block' materials for nanoscale science and technology, and have created great interest over the last two decades. Their one-dimensional geometry confers the potential for unique properties relevant to many applications[1–8]. Synthetic single-walled carbon nanotubes (CNTs), first prepared in 1991, are the most well-known SWNTs[1]. One of the main unsolved problems in CNT science is the covalent immobilization of functional moieties on their inner surfaces, which would allow a number of new ways to control the CNT properties and enable their use in 'molecular recognition' applications that exploit their 1-dimensional porosity (for example, catalysis, adsorption, membranes, sensors). The formation of covalent bonds at the CNT surface requires a transformation of carbon hybridization from sp^2 to sp^3. This can be accomplished on the outer surface by several methods, albeit with rather harsh reaction conditions[2–4]. However, the concave interior surface of CNTs leads to an extremely high thermodynamic barrier for this transformation, due to which the interior surfaces of CNTs have been considered to be essentially unreactive[2,5,6]. Although several examples of infiltration of the CNT channel with various types of atomic, molecular or nanoparticle species have been reported[6–8], as well as the modification of CNT tips with organic functional groups[2,9], to date there is no demonstration of the interior functionalization of CNTs via the formation of covalent bonds. Recent work has indicated that the interior surface of CNTs may become reactive under certain extreme conditions, further corroborating the practically unreactive nature of CNT inner walls[10,11].

Synthetic metal oxide nanotubes could potentially overcome the above limitation of CNTs. More specifically, synthetic aluminosilicate and aluminogermanate SWNTs[12–16] have attracted substantial interest in recent years. This type of nanotube consists of an octahedral aluminium(III) hydroxide outer wall and a tetrahedral silanol inner wall, with doubly-coordinated hydroxyl groups on the outer wall and pendant hydroxyls on the inner wall (Fig. 1a). The chemistry of such nanotube materials, which is based upon aqueous-phase synthesis under mild ($<100\,^{\circ}C$) conditions, has advanced considerably over the last decade. Single-walled and double-walled aluminogermanate analogues of the aluminosilicate SWNTs have been synthesized[17–19]. Detailed molecular-level insights on the mechanism of formation of these nanoscopic objects have been obtained[18,20], as well as the capability to engineer their shape and size with Ångstrom-level precision[21]. The first applications of these materials, for example, in the formation of high-quality polymer/nanotube membranes[22] and natural gas storage materials[23] have emerged recently.

The outer surfaces of the aluminosilicate SWNTs have been modified to a low degree via post-synthesis grafting with organosilane coupling agents[24]. However, this is a multi-step technique, which requires conversion of the aqueous SWNT gel into an anhydrous powder, and does not allow uniform distribution of the functionalizing agent along the length of the nanotube due to diffusion limitations induced by initial functionalization at the nanotube ends. These issues motivate the pursuit of a direct synthesis route for aluminosilicate SWNTs with organic functional groups immobilized at their interior surface. The key idea, as illustrated in Fig. 1b, is to (partially or completely) replace the siloxane reagent (Si-[O-R]$_4$, usually tetraethyl orthosilicate (TEOS)) in the bare aluminosilicate SWNTs with an organosiloxane reagent (R'-Si-[O-R]$_3$). This 'co-condensation' approach has been successful in the preparation of organic-functionalized microporous[24–27] and mesoporous[28,29] silicate materials. However, its application to nanotubes has been much more difficult, likely owing to the unique mechanisms operating in the synthesis of these

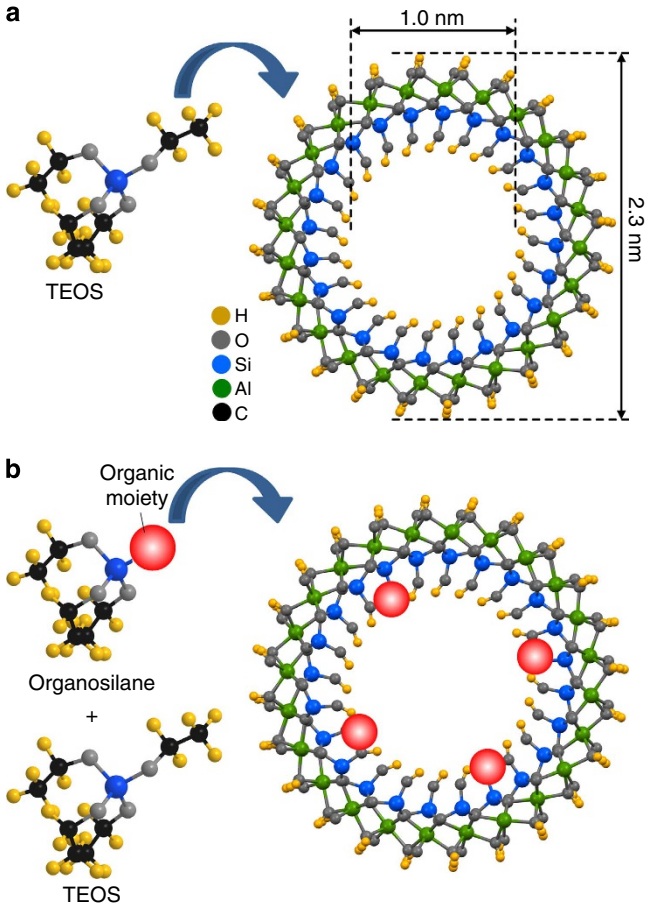

Figure 1 | Synthesis of aluminosilicate nanotubes. (**a**) Synthesizing bare aluminosilicate nanotubes using TEOS as the silicon source. (**b**) Forming nanotubes with organic moieties incorporated in their inner surfaces using a mixture of TEOS and a designed organosilane.

materials[20,21]. The first successful example of direct synthesis of organic-substituted aluminosilicate SWNTs involved the use of methyltriethoxysilane for producing methyl-functionalized aluminosilicate nanotubes[23]. However, the methyl group confers no additional functionality beyond increased hydrophobicity. Similar efforts using commercially available organosiloxane precursors with other functional groups (for example, aminopropyltriethoxysilane) have been unsuccessful.

Here we describe a direct, template-free, synthesis route for preparing functional single-walled amine-functionalized aluminosilicate nanotubes ('ANTs') with up to 15% of the interior ≡Si-OH groups substituted by ≡Si-CH_2NH_2 groups, via the use of a specifically synthesized precursor, aminomethyltriethoxysilane (AMTES). We hypothesize that the selection of the appropriate functional organosiloxane precursor is critical for the success of such an approach. Due to the small range of obtainable pore sizes (0.8–1 nm) of the SWNT and the confinement of the silanol groups in an ordered hydrogen-bonded network lining the pore[21], we hypothesize that avoiding steric effects is important. For example, the smallest commercially available aminosiloxane precursor, aminopropyltriethoxysilane, is too bulky and hydrophobic, and therefore is found to not incorporate successfully into the nanotube structure. We design and synthesize a novel functional precursor (AMTES) which satisfies the required criteria and leads to successful incorporation into the nanotube wall to yield the ANT material. The structure, morphology and surface chemistry of ANTs are investigated by a

range of solid-state characterization techniques, including conventional and cryogenic transmission electron microscopy (TEM/cryo-TEM), X-ray diffraction (XRD), nitrogen physisorption, elemental analysis, vibrational spectroscopy and solid-state NMR. The functionality of the primary amine groups in the interior of the SWNTs is assessed by CO_2, CH_4 and N_2 adsorption. The amine-functionalized nanotubes show a dramatic improvement in CO_2/CH_4 and CO_2/N_2 adsorptive selectivity over the bare nanotubes ('NTs'). The synthesis of amine-functionalized metal oxide SWNTs may facilitate a new class of functional SWNT materials obtainable by further chemical modifications of the amine groups.

Results

Morphology of amine-functionalized NTs. The morphology of the ANTs is evaluated by conventional and cryogenic TEM (Fig. 2). Low-resolution TEM images of both NTs and ANTs are shown in Fig. 2a. The ANTs show a smaller average length than the NTs (the average length of NT is 160 nm and of ANT 50 nm). The higher-resolution cryo-TEM images of NTs and ANTs (Fig. 2b) confirm the nanotubular structure of both materials. Electron diffraction (ED) was employed to investigate the crystallinity along the axis of NTs and ANTs (Fig. 2c). The ED patterns from both ANT and NT samples show an ordered nanotube wall structure. However, the NT reflections (006), (071) and (002) become less sharp, and reflections (004) and (063) are very weak or absent in the ED pattern of ANTs. The ED pattern from the post-synthesis functionalized nanotubes (Supplementary Fig. 1)[30], in which the organic moieties are likely immobilized at the pore mouth, is nearly identical to the pattern from the bare NT. These observations indicate successful random substitution of AMTES in the nanotube inner wall.

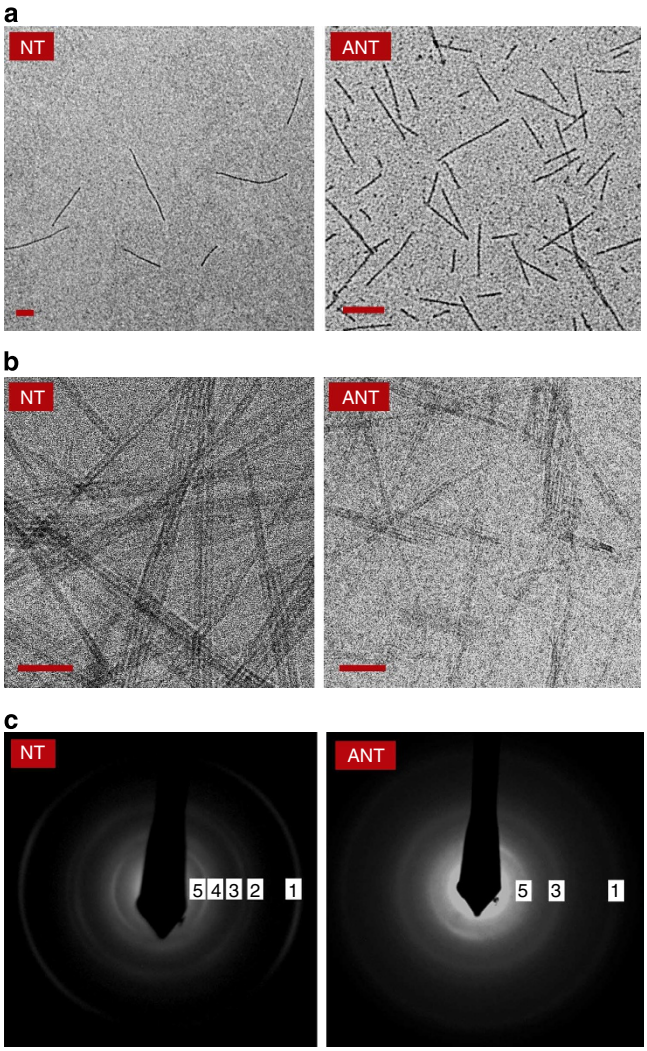

Figure 2 | Characterization of NTs and ANTs by TEM and ED. (**a**) Conventional and (**b**) cryo-TEM images. (**c**) ED patterns of NTs and ANTs. The scale bar for the conventional TEM images represents 20 nm, and for cryo-TEM images 10 nm. The reflections numbered 1–5 in the ED patterns are assigned to (006), (004), (063), (071) and (002).[14]

Interior surface properties. The interior surface properties of the ANTs are comprehensively evaluated by a combination of N_2 physisorption, ^{13}C solid-state NMR, Fourier transform (FT)-Raman spectroscopy and elemental analysis. N_2 physisorption is an excellent tool to estimate the expected pore volume reduction due to the AMTES substitution for the ANT synthesis. The raw physisorption isotherms and the deduced pore size distributions and micropore surface areas are presented in Fig. 3. The lower pore volume of ANTs and the occurrence of the maximum in the pore size distribution at a smaller pore size (8.7 Å for ANTs versus 9.5 Å for NTs), are both due to the larger size of the immobilized $\equiv$Si-CH_2NH_2 group in comparison with the $\equiv$Si-OH group in the NTs. Given the volumes of the hydroxyl and the aminomethyl groups (16.9 and 38.1 $Å^3$, as estimated from the atomic van der Waals radii), the fractional organic substitution ratio in the ANTs can be calculated by comparing the micropore volumes of the NTs and ANTs. The derived fractional organic substitution is 0.16, which is close to the AMTES:TEOS ratio (0.2) used in the ANT synthesis. The atomic compositions derived from elemental analysis are summarized in Supplementary Table 1, and the raw elemental analysis data are presented in Supplementary Table 2. First, the identical Si:Al ratio (0.5) in both the ANTs and NTs rules out the presence of impurities caused by possible self-polymerization of AMTES and TEOS during the synthesis. Second, the nitrogen and carbon signals are only observed in ANTs, thereby showing the presence of the organic moieties in the sample. The fractional organic substitution estimated from the carbon signal is 0.16, and from the nitrogen signal is 0.11, broadly consistent with the quantification from N_2 physisorption (0.16).

Although N_2 physisorption and elemental analysis suggest the presence of immobilized organic moieties in the ANT, ^{13}C solid-state NMR and FT-Raman spectroscopy identify the organic species. The single peak at 27 p.p.m. in the ^{13}C NMR spectrum (Fig. 4a) of the ANT is assigned to the aminomethyl group. The absence of peaks from the ethoxy groups (57 p.p.m. for -OCH_2- and 17 p.p.m. for -CH_3)[31] of the reagent AMTES provides clear support for the success of the ANT synthesis. When using TEOS for NT synthesis, the ethoxy groups are hydrolysed and a Q^3(6Al) $\equiv$Si-OH coordination environment is formed[15,20,30]. This coordination is exclusively found in the aluminosilicate NT material. An identical hydrolysis of ethoxy groups and formation of an equivalent T^3(6Al) $\equiv$Si-CH_2NH_2 environment[15,30] is clear evidence of the formation of the aminomethylsilane-substituted single-walled aluminosilicate NTs (ANTs). The FT-Raman spectra for both NTs and ANTs are shown in Fig. 4b. The additional peaks (1,298, 1,450, 1,506 and 2,950 cm^{-1}) seen in the ANT material, in comparison with the NT material, are assigned to C-N stretching, C-H deformation, C-N deformation and C-H stretching vibrations, respectively[32]. These vibrational modes further confirm the presence of the aminomethyl groups in the ANT material.

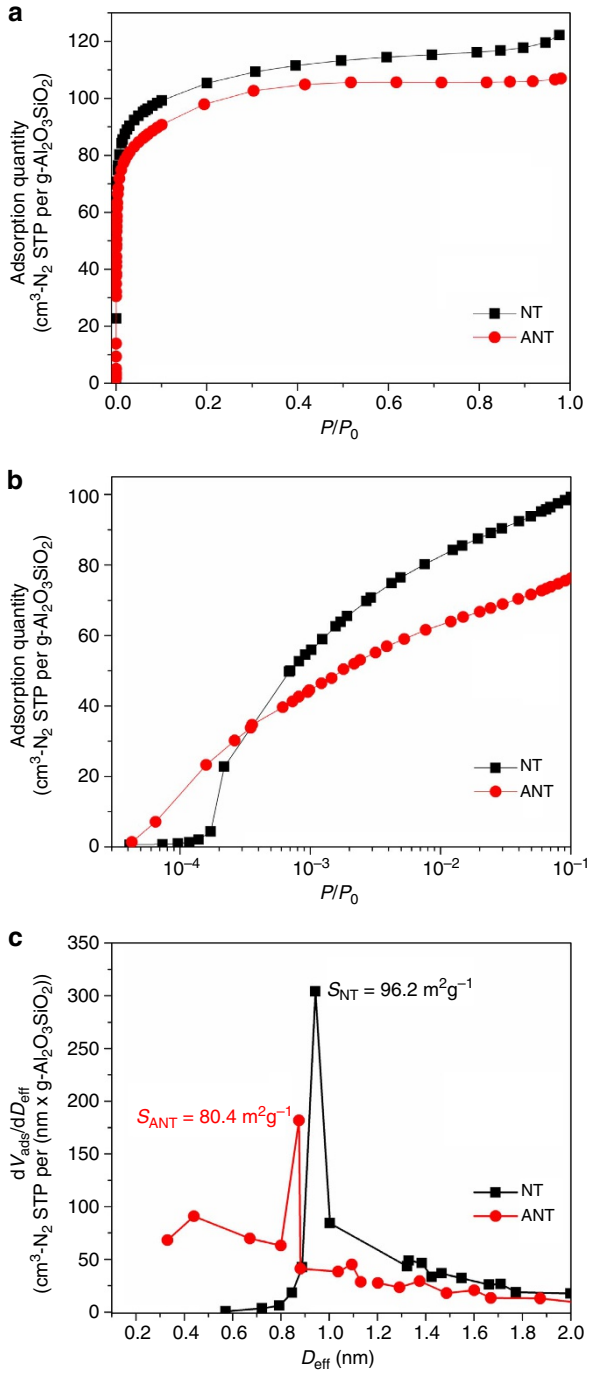

Figure 3 | Porosity characterization of NTs and ANTs using N_2 physisorption. (**a**) Full isotherms on a linear scale. (**b**) Isotherms on semilog scale to highlight the low-pressure region. (**c**) Pore size distributions and *t*-plot micropore surface areas derived from the physisorption isotherms.

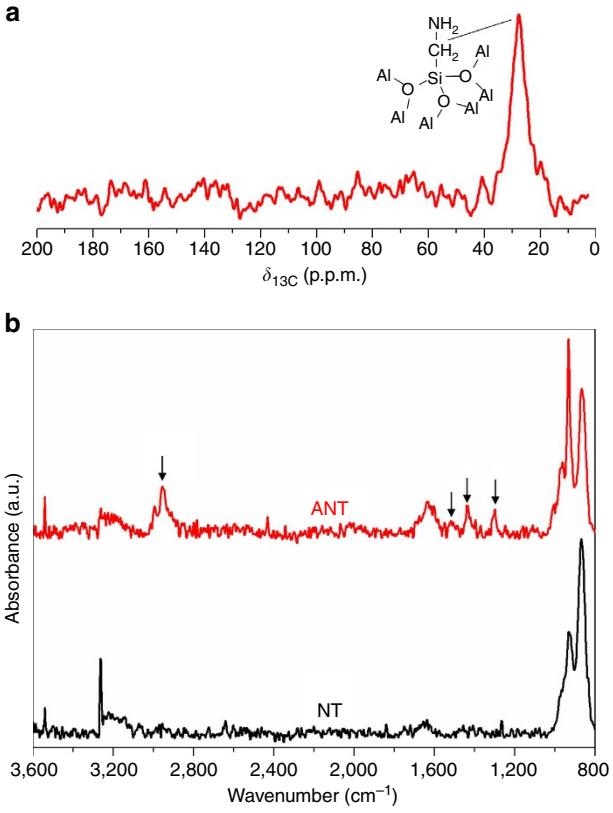

Figure 4 | Interior surface properties of NTs and ANTs. (**a**) ^{13}C solid-state NMR spectrum of ANT. (**b**) FT-Raman spectra of NT and ANT. The arrows identify peaks assigned to C-N and C-H vibrations in the ANT sample.

Silicon coordination. The Si coordination in the ANTs is rigorously assessed by ^{29}Si and ^{27}Al NMR. ^{29}Si direct polarization NMR spectra are shown in Fig. 5a. For both NTs and ANTs, the peak at -79 p.p.m. is known as the Q^3(6Al) ≡Si-OH fingerprint[15,20,30] and originates from the use of TEOS as a Si source in both cases. The peak at -57 p.p.m., observed only in ANTs but not in NTs, occurs from the additional Si source (AMTES) used in ANT synthesis. According to the aforementioned discussion regarding the absence of the ethoxy groups, the peak at -57 p.p.m. could be assigned to either T^3(3Si) or T^3(6Al) Si, wherein T^3(3Si) would be due to self-polymerization of AMTES and T^3(6Al) would be the fingerprint of isolated aminomethylsilane groups in the ANTs. To differentiate between these two possibilities, a control experiment was performed by immobilization of AMTES on a mesoporous silica support (SBA-15), resulting in a combination of T^1(1Si), T^2(2Si), and T^3(3Si) coordination (the raw ^{29}Si NMR spectrum is shown in Supplementary Fig. 2). The ^{29}Si chemical shift of the T^3(3Si) silicon was found at -72 p.p.m., which is quite different from the -57 p.p.m. chemical shift seen in the ANTs. Hence, the peak at -57 p.p.m. is very likely due to the isolated ≡Si-CH_2NH_2 aminomethylsilane groups in the ANTs. Another supporting evidence for the peak assignment is that when using methytriethoxysilane (MTES) as the reagent, there is only a 2 p.p.m. difference between the T^0 (neat reagent in solution state, -41 p.p.m.) and T^3(6Al) ≡Si-CH_3 peak (isolated methylsilane groups in the NT, -43 p.p.m.)[23]. In our AMTES system (Supplementary Table 3), a similar 2 p.p.m. difference is also observed for T^0 (-55 p.p.m., Supplementary Fig. 3) and T^3(6Al) (-57 p.p.m.). Provided that the repetition delay is chosen to be long enough, the integrated areas under the -57 p.p.m. and -79 p.p.m. Si peaks in the direct polarization NMR spectrum can be used for quantifying the fractional substitution of ≡Si-CH_2NH_2 for ≡Si-OH groups. For the ANT sample, this quantity is determined to be 0.18. The ^{27}Al spectra of NTs and ANTs are nearly identical (Fig. 5b). The peak at -4 p.p.m. is due to the octahedral Al coordination in both nanotubes. The quantification of the fractional substitution of T^3(6Al) for Q^3(6Al) by various techniques is shown in this work (Supplementary Table 4). The average fractional substitution from all the analytical techniques is 0.15. The fractional substitution derived from the elemental analysis represents the

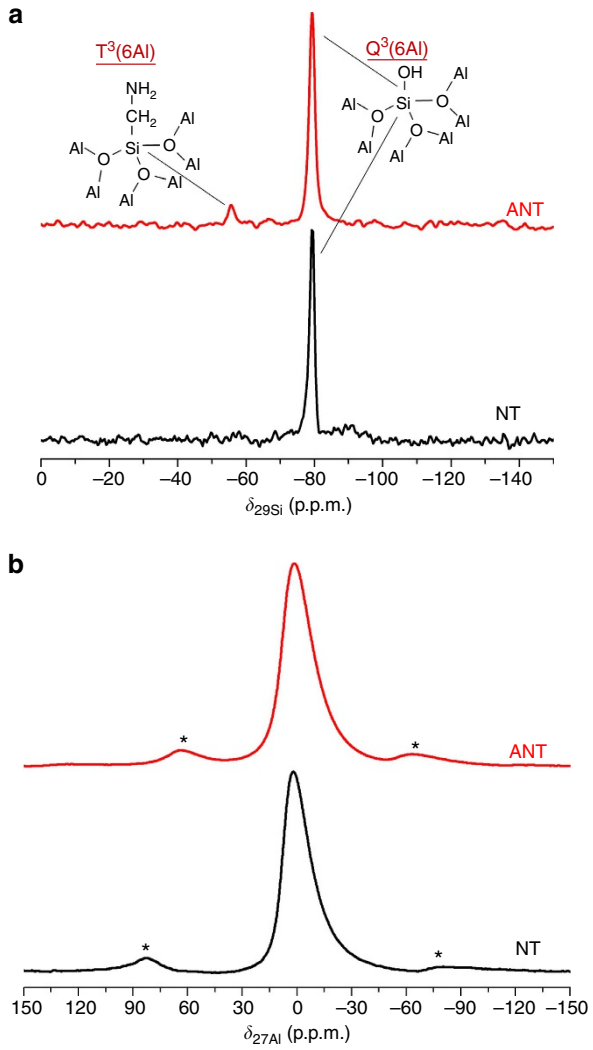

Figure 5 | Solid-state NMR spectra of NTs and ANTs. (**a**) ^{29}Si direct polarization and (**a**) ^{27}Al solid-state NMR spectra of NTs and ANTs. The asterisks denote the spinning side bands.

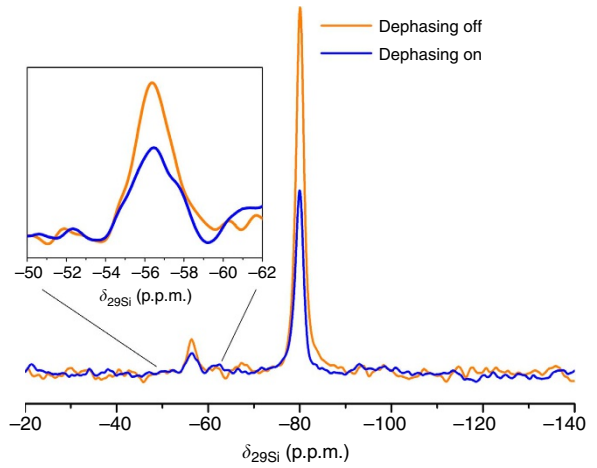

Figure 6 | ^{29}Si/^{27}Al TRAPDOR NMR spectra of the ANT material. The two spectra obtained from the ^{29}Si/^{27}Al TRAPDOR sequence in the presence (blue) and absence (orange) of the dephasing pulse.

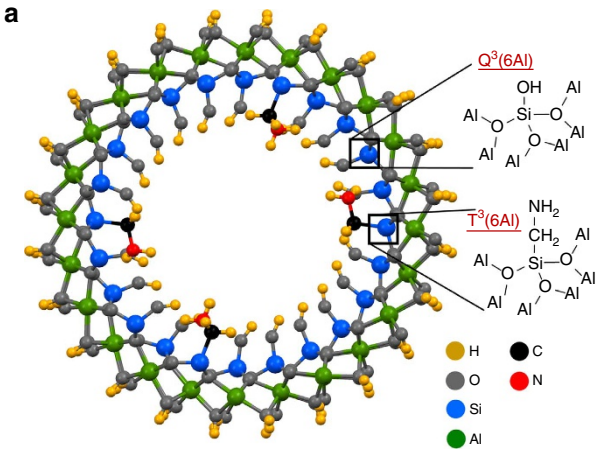

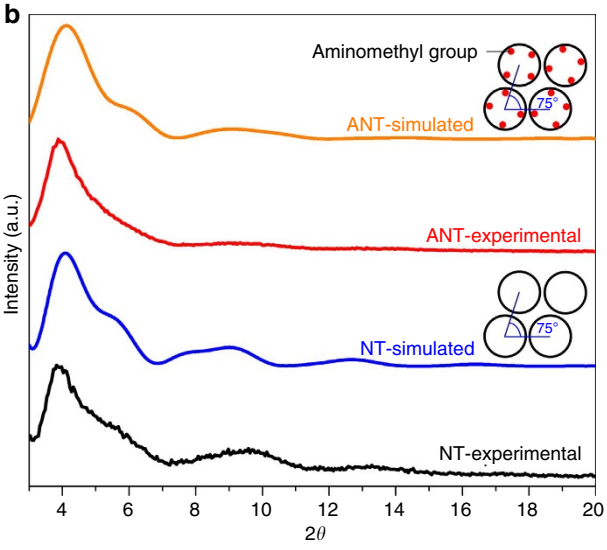

Figure 7 | Structural model and XRD simulations of NTs and ANTs. (**a**) Proposed structural model of ANT. (**b**) Measured and simulated XRD patterns of NTs and ANTs.

organic moiety immobilized on both interior and external surface of ANTs whereas the values deduced from the ^{29}Si solid-state NMR and N_2 physisorption represent the amine moiety grafted only on the interior surface of ANTs.

To gain more insight into the connectivity between Si (from both TEOS and AMTES as Si sources) and Al atoms in the ANT wall, ^{29}Si/^{27}Al transfer of populations in double resonance (TRAPDOR) experiments were employed[33]. The TRAPDOR technique directly probes the dipolar coupling between a spin = 1/2 nucleus (^{29}Si) and a spin > 1/2 nucleus (^{27}Al), and thereby characterizes the proximity of these two nuclei[33,34]. Practically speaking, in the presence of a dephasing pulse from the ^{27}Al channel, the ^{29}Si peak intensity will be reduced if the Si atoms are within a few Angstroms of the Al atoms[33,34]. The TRAPDOR spectra for the ANT are shown in Fig. 6. A clear intensity reduction is observed for both Q^3(6Al) and T^3(6Al) peaks in the presence of the ^{27}Al dephasing pulse, confirming the close proximity between Al and Si atoms and therefore our peak assignment. On the other hand, a control sample composed of a physical mixture of mesoporous silica (SBA-15) and α-alumina is also measured (Supplementary Fig. 4). No intensity reduction of the Si signal is observed due to a lack of silicon-aluminium connectivity.

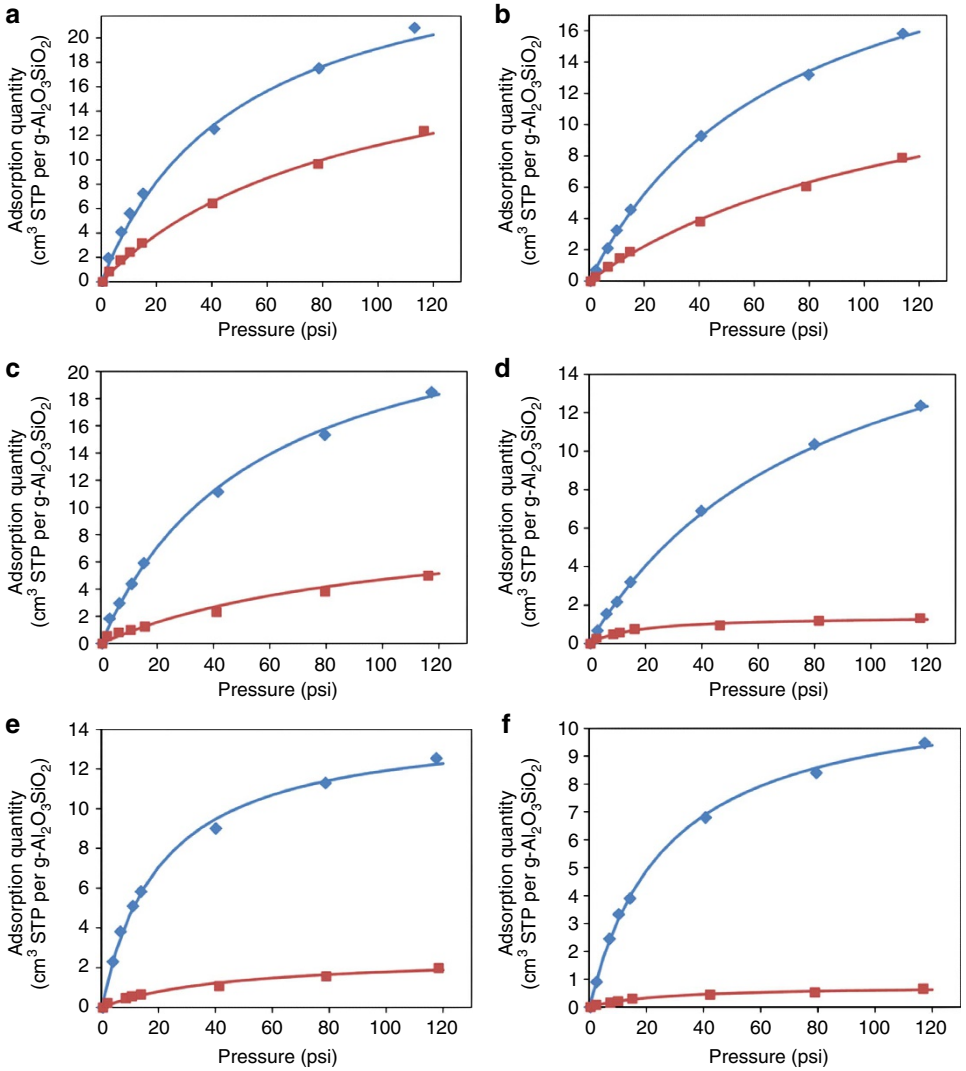

Figure 8 | CO_2 and CH_4 adsorption isotherms of NT and ANT materials. The adsorption isotherms of (**a**) CO_2 at 25 °C, (**b**) CO_2 at 67 °C, (**c**) CH_4 at 25 °C, (**d**) CH_4 at 67 °C, (**e**) N_2 at 25 °C and (**f**) N_2 at 67 °C for NT (blue diamonds) and ANT (red squares); and the fitted curves (solid lines) to the Langmuir model.

Structural modelling. On the basis of the interior surface chemistry and framework characterizations, a structural model of the ANT was constructed (Fig. 7a). Using the structural models of the NT and ANT materials, XRD simulations were then performed. The comparison of the simulated and experimental XRD patterns for NTs and ANTs is summarized in Fig. 7b. As discussed in our previous works[15,22], the XRD patterns for NTs are not dominated by Bragg diffraction but by scattering from small bundles of NTs. In particular, both computational and experimental evidence shows that the NTs form small bundles of three or four individual nanotubes. The XRD pattern is fully explained by the scattering form factor of a bundle composed of three or four tubular objects[35]. The immobilization of the aminomethyl groups at the inner surface of the nanotubes causes a deviation in the form factor from the plain NTs, which describes an ideal core-shell cylindrical object with uniform scattering length density. This subtle difference between NTs and ANTs is successfully captured in both experimental and simulated XRD patterns, wherein the ANT shows less prominent features in the regions of 5–6°, 8–10° and 12–14° 2θ. The excellent agreement between experimental and computational XRD patterns for ANT further demonstrates the successful synthesis of ANTs. Although nanotube synthesis with 20% AMTES substitution for TEOS successfully yielded ANTs with 15% T^3(6Al) substitution for Q^3(6Al) in the nanotube wall, we are so far unable to synthesize ANTs with 50 and 100% AMTES substitution (Supplementary Figs 5–7). To further advance the synthesis of organic-functionalized single-walled metal oxide NTs, a better understanding of the molecular-level events occurring during the synthesis is necessary[20,21].

Gas adsorption. Single-component gas adsorption measurements via quartz crystal microbalance-based techniques[36] were performed to evaluate the functionality of the ANT material. The CO_2/N_2 and CO_2/CH_4 molecular pairs were chosen to assess the effect of the aminomethyl groups on adsorptive selectivity for CO_2, which is relevant to carbon capture from flue gas and natural gas purification[37,38]. The full adsorption isotherms are shown in Fig. 8, and the ideal adsorption selectivity of NTs and ANTs is summarized in Fig. 9. In this work, the ideal adsorption selectivity is defined in the standard manner, as the ratio of the single-component adsorption uptakes of two different adsorbate molecules at the same partial pressure. As shown in Fig. 9, ANTs with a 15% aminomethyl group substitution for hydroxyls exhibit a dramatic improvement in selectivity over the bare NTs for both CO_2/CH_4 (up to four-fold increase) and CO_2/N_2 (up to ten-fold increase).

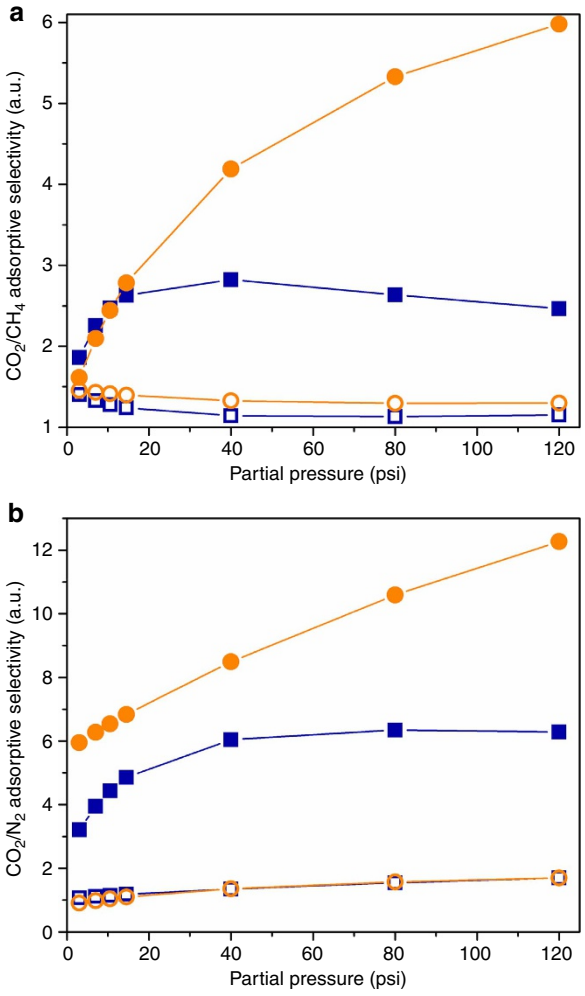

Figure 9 | Ideal CO_2 adsorption selectivity of NT and ANT materials. Ideal CO_2 adsorption selectivity of NTs (open symbols) and ANTs (closed symbols), for gas pairs of (**a**) CO_2/CH_4 and (**b**) CO_2/N_2, at 25 °C (squares) and 67 °C (circles).

Discussion

To gain more insight into the observed selectivity enhancements and evaluate the affinity of the ANT and NT walls for the adsorbate molecules, the Henry's constants for adsorption in each nanotube material were obtained from fits of the full isotherms to the Langmuir model (Supplementary Note 1). The Henry's constant ratios between ANTs and NTs (K_{ANT}/K_{NT}) are summarized in Supplementary Table 5. The detailed Langmuir fitting parameters are presented in Supplementary Table 6. In general, the Henry's constants decrease for all the adsorbates when partially replacing surface hydroxyl groups with aminomethyl groups. As expected, the isolated aminomethyl ($\equiv$Si-CH_2NH_2) groups in the ANTs possess overall weaker affinities for the adsorbates in comparison with the hydroxyl ($\equiv$Si-OH) groups. However, the aminomethyl groups greatly suppress the adsorption of CH_4 and N_2 in relation to CO_2, thereby leading to a large enhancement in CO_2/CH_4 and CO_2/N_2 adsorption selectivity. Furthermore, the relative suppression in CH_4 and N_2 adsorption becomes more efficient when the temperature is increased from 25 °C to 67 °C, as well as by increasing the pressure, thereby leading to increased adsorption selectivity with both temperature and pressure. Previous computational and experimental works suggest that single-walled carbon nanotubes of comparable diameter (~1 nm) have a maximum CO_2/CH_4 and CO_2/N_2 adsorption selectivity of about 7 at 25 °C and a low pressure of 1 atm, with the selectivity declining as pressure increases, for example, to about 5.5 at 8 bar (~120 psi)[39,40]. More importantly, in the case of carbon nanotubes there is no available route for controlling these properties by functionalizing or modifying their interior surfaces.

The smaller reduction of Henry's constant for CO_2 is due to the mechanism of amine group binding to CO_2 molecules. It is well known that one equivalent of a free base moiety—typically water—is needed for a primary amine to adsorb one equivalent of CO_2[41,42]. However, under anhydrous conditions such as in the present adsorption measurements, two adjacent primary amines are required to adsorb one equivalent of CO_2. The primary amine groups are expected to be distributed in a random manner at the inner surface of the ANTs, and there is no evidence available for preferred clustering (or non-clustering) of the aminomethylsilane functional sites. At a 15% substitution of silanol groups by aminomethyl groups in the confined space of the inner nanotube wall, we expect the presence of isolated amine sites as well as amine groups in close proximity to each other. Given the adsorption mechanisms discussed above, amine groups in close proximity will provide a positive contribution to CO_2 adsorption, whereas an isolated amine would likely show lower CO_2 affinity than the surface hydroxyls. These two competing effects, present only for CO_2 adsorption but not for CH_4 and N_2, are likely to be the key factor leading to a relatively small reduction of Henry's constant for CO_2 and the high CO_2/CH_4 and CO_2/N_2 selectivity in ANTs.

In conclusion, through a single-step approach, we have successfully synthesized single-walled aminoaluminosilicate nanotubes (ANTs) with a 15% aminomethyl group substitution for the hydroxyl groups on the interior nanotube wall. A combination of characterization techniques including TEM, cryo-TEM, ^{13}C, ^{29}Si and ^{27}Al solid-state NMR, FT-Raman spectroscopy, elemental analysis, nitrogen physisorption and XRD measurements and simulations, have yielded conclusive structural information on the ANTs at the molecular level. CO_2, CH_4 and N_2 adsorption measurements on the bare NTs and amine-functionalized ANTs have demonstrated that the interior surface properties can be significantly tailored by the incorporation of the primary amines. The modified interior surface results in dramatically enhanced CO_2/CH_4 and CO_2/N_2 ideal adsorption selectivity. This work elucidates the fabrication of functionalized single-walled metal-oxide nanotube materials with altered interior surface properties. Such an approach to synthesize functional nanotube materials can enable a wider range of applications for nanotubes, which have so far been inaccessible to other nanotube systems such as carbon nanotubes.

Methods

Synthesis of aminomethyltriethoxysilane. AMTES was synthesized by treating the commercially available chloromethyltriethoxysilane with gaseous ammonia using a Parr reactor. The reaction was performed anhydrously at 900–1,000 psi and 100 °C for 5 h. The synthesis details were identical to that described in our previous work.[43]

Nanotube synthesis. TEOS and AMTES were mixed with aluminium-tri-sec-butoxide in a glove box filled with nitrogen. The mixture, with a TEOS:AMTES:Al:$HClO_4$ molar ratio of $(1-x)$:x:2:1, was added into a Teflon jar (1,000 ml capacity) containing 500 ml of 38 mM perchloric acid. Bare aluminosilicate nanotubes ('NTs') were obtained when $x=0$; whereas ANTs were synthesized when $x=0.2$. Synthesis products with $x=0.5$ and 1 are discussed in the Supplementary Figs 5–7. The aqueous mixture was vigorously stirred at room temperature in ambient conditions for 24 h. The solution was then diluted with deionized water water by a factor of 3.8 with respect to volume, and then stirred at 95 °C for 96 h. Once the temperature was brought to 95 °C, the solution turned from cloudy to clear in about 1 h. After the solution was cooled to room

temperature, a 30 wt% ammonia solution was added dropwise until gelation of the suspended nanotubes occurred. The gel was isolated by centrifugation at 7,000 r.p.m. for 10 min. The supernatant was discarded and a few drops of 10 N hydrochloric acid were added to the gel, thereby re-dispersing the nanotubes. The gel was dialyzed against 10 wt% ammonium hydroxide solution for 24 h and then against deionized water water for 3 days, using a dialysis membrane with a 15 kDa molecular weight cutoff. To obtain powder samples, the purified gel was dried at 60 °C and then ground lightly to disperse the agglomerated nanotubes. Approximately 1 g of powder sample is obtained from a 1 l synthesis batch volume.

Transmission electron microscopy. TEM images were collected using a JEOL JEM-2200FS 200 kV field emission transmission electron microscope with an in-column Omega energy filter (operated at 200 kV). Detailed sample preparation procedures are described in our previous work[21]. Cryo-TEM images were recorded at the Apkarian Integrated Electron Microscopy Core (Emory University) using a JEOL JEM-1210 microscope operated at 100 kV[15].

X-ray diffraction measurements and simulations. XRD measurements in Bragg–Brentano geometry were performed on a PAnalytical X'pert Pro MPD diffractometer operating with a Cu Kα source. Diffraction data were collected with a collimator and proportional (Miniprop) He-filled detector, in the range of 3–30° 2θ and a step size of 0.05° 2θ. The Reflex module of the Materials Studio 3.2 package (Accelrys) was used for XRD pattern simulations, and the methodological details have been reported in our previous work[15].

Nitrogen physisorption. Nitrogen physisorption measurements were carried out on a Micromeritics Tristar II at 77 K. The sample was placed in an analysis tube and degassed under 15 mTorr at 200 °C for 12 h before physisorption measurements.

Solid-state NMR. The ^{13}C, ^{27}Al and ^{29}Si MAS NMR measurements were carried out on a Bruker DSX 300 using a 7 mm rotor. For ^{13}C cross-polarization MAS NMR, the sample was spun at 5 kHz, and a single $\pi/2$ pulse with a duration of 5 μs and a repetition time of 4 s was used. The sample was spun at 5–6 kHz for ^{27}Al MAS NMR, for which a single pulse of $\pi/6$ (duration 0.6 μs) and a repetition time of 0.1 s was used. For ^{29}Si MAS NMR, direct polarization scans were performed with repetition times of 10 s at $\pi/2$ single pulse (duration 5 μs) and 5 kHz spinning rate. The chemical shifts of ^{13}C, ^{27}Al and ^{29}Si were referenced to adamantane (^{13}C chemical shift at 38.45 p.p.m.), an aqueous solution of aluminium trichloride (^{27}Al chemical shift at 0 p.p.m.), and solid 3-(trimethylsilyl)-1-propanesulphonic acid sodium salt (^{29}Si chemical shift at 0 p.p.m.), respectively. The $^{29}Si/^{27}Al$ Transfer of Populations in Double Resonance (TRAPDOR) NMR experiments were carried out on a Bruker Avance III 400 using a triple resonance probe equipped for 3.2 mm MAS rotors. The pulse sequence followed the previous literature using decoupling of the ^{27}Al-nucleus during the evolution period[33]. The MAS spinning speed was set to 5 kHz. A dephasing time of 2 ms (10 rotor periods) was applied for the ^{27}Al decoupling with a frequency of ~100 kHz.

Raman spectroscopy. FT-Raman spectra were obtained on a Bruker Vertex 80v spectrometer with dual FTIR and FT-Raman benches and CaF_2 beamsplitter. Elemental analysis was performed by Columbia Analytical Services, Inc.

Gas adsorption measurements. Adsorption measurements were performed with a quartz crystal microbalance-based measurement apparatus developed in-house[36]. For the sample preparation, the as-synthesized NT or ANT gel was drop-coated by depositing a few drops on the quartz crystal microbalance substrate. The substrates were then pre-baked in an oven at 110 °C and atmospheric pressure for 30 min. The samples were then mounted in the measurement apparatus and degassed *in situ* at 180 °C and 4 mTorr for about 24 h before adsorption measurements. Single-component adsorption isotherms of CO_2, CH_4 and N_2 in the two types of NTs were then collected at 25 °C and 67 °C and pressures ranging from 0.3–120 psi (about 8 atm). Measurements were taken in pressure intervals of 2–3 psi (below 1 atm) and ~40 psi (above 1 atm).

References

1. Iijima, S. Helical microtubules of graphitic carbon. *Nature* **354,** 56–58 (1991).
2. Singh, P. *et al.* Organic functionalisation and characterisation of single-walled carbon nanotubes. *Chem. Soc. Rev.* **38,** 2214–2230 (2009).
3. Ma, P. -C. *et al.* Dispersion and functionalization of carbon nanotubes for polymer-based nanocomposites: a review. *Compos. Part A* **41,** 1345–1367 (2010).
4. Karousis, N. *et al.* Current progress on the chemical modification of carbon nanotubes. *Chem. Rev.* **110,** 5366–5397 (2010).
5. Kuzmany, H. *et al.* Functionalization of carbon nanotubes. *Synth. Met.* **141,** 113–122 (2004).
6. Vairavapandian, D. *et al.* Preparation and modification of carbon nanotubes: review of recent advances and applications in catalysis and sensing. *Anal. Chim. Acta* **626,** 119–129 (2008).
7. Singh, S. *et al.* Carbon nanotube surface science. *Int. J. Nanotechnol.* **5,** 900–929 (2008).
8. Yanagi, K. *et al.* Photosensitive function of encapsulated dye in carbon nanotubes. *J. Am. Chem. Soc.* **129,** 4992–4997 (2007).
9. Majumder, M. *et al.* Mass transport through carbon nanotube membranes in three different regimes: ionic diffusion and gas and liquid flow. *ACS Nano* **5,** 3867–3877 (2011).
10. Chamberlain, T. W. *et al.* Reactions of the inner surface of carbon nanotubes and nanoprotrusion processes imaged at the atomic scale. *Nature Chem.* **3,** 732–737 (2011).
11. Giambastiani, G. *et al.* Functionalization of multiwalled carbon nanotubes with cyclic nitrones for materials and composites: addressing the role of CNT sidewall defects. *Chem. Mater.* **23,** 1923–1938 (2011).
12. Wada, S. I. *et al.* Synthetic allophane and imogolite. *J. Soil Sci.* **30,** 347–352 (1979).
13. Barron, P. F. *et al.* Detection of imogolite in soils using solid-state Si-29 NMR. *Nature* **299,** 616–618 (1982).
14. Mukherjee, S. *et al.* Phenomenology of the growth of single-walled aluminosilicate and aluminogermanate nanotubes of precise dimensions. *Chem. Mater.* **17,** 4900–4909 (2005).
15. Kang, D. -Y. *et al.* Dehydration, dehydroxylation, and rehydroxylation of single-walled aluminosilicate nanotubes. *ACS Nano* **4,** 4897–4907 (2010).
16. Theng, B. K. G. *et al.* Surface-properties of allophane, halloysite, and imogolite. *Clays Clay Miner.* **30,** 143–149 (1982).
17. Mukherjee, S. *et al.* Short, highly ordered, single-walled mixed-oxide nanotubes assemble from amorphous nanoparticles. *J. Am. Chem. Soc.* **129,** 6820–6826 (2007).
18. Levard, C. *et al.* Formation and growth mechanisms of imogolite-like aluminogermanate nanotubes. *Chem. Mater.* **22,** 2466–2473 (2010).
19. Maillet, P. *et al.* Growth kinetic of single and double-walled aluminogermanate imogolite-like nanotubes: an experimental and modeling approach. *Phys. Chem. Chem. Phys.* **13,** 2682–2689 (2011).
20. Yucelen, G. I. *et al.* Formation of single-walled aluminosilicate nanotubes from molecular precursors and curved nanoscale intermediates. *J. Am. Chem. Soc.* **133,** 5397–5412 (2011).
21. Yucelen, G. I. *et al.* Shaping single-walled metal oxide nanotubes from precursors of controlled curvature. *Nano. Lett.* **12,** 827–832 (2012).
22. Kang, D. -Y. *et al.* Single-walled aluminosilicate nanotube/poly(vinyl alcohol) nanocomposite membranes. *ACS Appl. Mater. Interfaces* **4,** 965–976 (2012).
23. Bottero, I. *et al.* Synthesis and characterization of hybrid organic/inorganic nanotubes of the imogolite type and their behaviour towards methane adsorption. *Phys. Chem. Chem. Phys.* **13,** 744–750 (2011).
24. Zanzottera, C. *et al.* Physico-chemical properties of imogolite nanotubes functionalized on both external and internal surfaces. *J. Phys. Chem. C* **116,** 7499–7506 (2012).
25. Jones, C. W. *et al.* Organic-functionalized molecular sieves as shape-selective catalysts. *Nature* **393,** 52–54 (1998).
26. Tsuji, K. *et al.* Organic-functionalized molecular sieves (OFMSs) I. Synthesis and characterization of OFMSs with polar functional groups. *Microporous Mesoporous Mater.* **29,** 339–349 (1999).
27. Jones, C. W. *et al.* Organic-functionalized molecular sieves (OFMSs). II. Synthesis, characterization and the transformation of OFMSs containing non-polar functional groups into solid acids. *Microporous Mesoporous Mater.* **33,** 223–240 (1999).
28. Stein, A. *et al.* Hybrid inorganic-organic mesoporous silicates—Nanoscopic reactors coming of age. *Adv. Mater.* **12,** 1403–1419 (2000).
29. Hoffmann, F. *et al.* Silica-based mesoporous organic-inorganic hybrid materials. *Angew. Chem. Int. Ed. Engl.* **45,** 3216–3251 (2006).
30. Kang, D. Y. *et al.* Single-walled aluminosilicate nanotubes with organic-modified interiors. *J. Phys. Chem. C* **115,** 7676–7685 (2011).
31. Ek, S. *et al.* A Si-29 and C-13 CP/MAS NMR study on the surface species of gas-phase-deposited gamma-aminopropylalkoxysilanes on heat-treated silica. *J. Phys. Chem. B* **108,** 11454–11463 (2004).
32. Socrates, G. *Infrared and Raman Characteristic Group Frequencies: Tables and Charts* 3rd edn (Wiley, 2001).
33. Grey, C. P. *et al.* Determination of the quadrupole coupling constant of the invisible aluminum spins in Zeolite HY with $^1H/^{27}Al$ TRAPDOR NMR. *J. Am. Chem. Soc.* **117,** 8232–8242 (1995).
34. Holland, G. P. & Alam, T. M. Location and orientation of adsorbed molecules in zeolites from solid-state REAPDOR NMR. *Phys. Chem. Chem. Phys.* **7,** 1739–1742 (2005).
35. Cambedouzou, J. *et al.* On the diffraction pattern of C-60 peapods. *Eur. Phys. J. B* **42,** 31–45 (2004).
36. Venkatasubramanian, A. *et al.* Gas Adsorption characteristics of metal–organic frameworks via quartz crystal microbalance techniques. *J. Phys. Chem. C* **116,** 15313–15321 (2012).

37. Tagliabue, M. *et al.* Natural gas treating by selective adsorption: material science and chemical engineering interplay. *Chem. Eng. J.* **155,** 553–566 (2009).
38. Bollini, P. *et al.* Oxidative degradation of aminosilica adsorbents relevant to postcombustion CO_2 capture. *Energy Fuels* **25,** 2416–2425 (2011).
39. Lithoxoos, G. P. *et al.* Adsorption of N_2, CH_4, CO and CO_2 gases in single walled carbon nanotubes: a combined experimental and Monte Carlo molecular simulation study. *J. Supercrit. Fluids* **55,** 510–523 (2010).
40. Razavi, S. *et al.* Modeling the adsorptive selectivity of carbon nanotubes for effective separation of CO_2/N_2 mixtures. *J. Mol. Model* **17,** 1163–1172 (2011).
41. Choi, S. *et al.* Adsorbent materials for carbon dioxide capture from large anthropogenic point sources. *ChemSusChem.* **2,** 796–854 (2009).
42. Bollini, P. *et al.* Amine-oxide hybrid materials for acid gas separations. *J. Mater. Chem.* **21,** 15100–15120 (2011).
43. Brunelli, N. A. *et al.* Tuning cooperativity by controlling the linker length of silica-supported amines in catalysis and CO_2 capture. *J. Am. Chem. Soc.* **134,** 13950–13953 (2012).

Acknowledgements

This work was supported by Phillips 66 Company and the National Science Foundation (CAREER, CBET-0846586). The authors acknowledge Prof. E.R. Wright (Emory University) for access to cryo-TEM facilities.

Author contributions

D.-Y.K., C.W.J. and S.N. conceived the research. D.-Y.K. and N.A.B. prepared all the nanotube samples, performed precursor synthesis and collected the FT-Raman spectra. D.-Y.K. conducted the N_2 physisorption measurements and XRD measurements and simulations and collected the ED patterns. J.Z. assisted with constructing the nanotube models for the XRD simulations. D.-Y.K. and J.L. carried out the NMR experiments and data analysis. G.I.Y. collected the TEM images. A.V. performed the gas adsorption measurements. D.-Y.K., A.V., N.A.B., C.W.J., S.N. and P.J.H. contributed to the adsorption data interpretation. D.-Y.K., C.W.J. and S.N. wrote the manuscript and all authors participated in manuscript editing.

Additional information

Supplementary Information accompanies this paper at http://www.nature.com/naturecommunications

Competing financial interests: The authors declare no competing financial interests.

Reprints and permission information is available online at http://npg.nature.com/reprintsandpermissions/

How to cite this article: Kang, D.-Y. *et al.* Direct synthesis of single-walled aminoaluminosilicate nanotubes with enhanced molecular adsorption selectivity. *Nat. Commun.* 5:3342 doi: 10.1038/ncomms4342 (2014).